Comparative Analysis of Surface-Enhanced Raman Spectroscopy of Daidzein and Formononetin

ARTICLE *in* THE JOURNAL OF PHYSICAL CHEMISTRY B · MAY 2010

Impact Factor: 3.3 · DOI: 10.1021/jp101389t · Source: PubMed

5 AUTHORS, INCLUDING:

Ryo Sekine
Centre for Ecology & Hydrology
22 PUBLICATIONS **79** CITATIONS
SEE PROFILE

Jitraporn Vongsvivut
Australian Synchrotron
33 PUBLICATIONS **178** CITATIONS
SEE PROFILE

Evan G Robertson
La Trobe University
95 PUBLICATIONS **1,782** CITATIONS
SEE PROFILE

Leone Spiccia
Monash University (Australia)
376 PUBLICATIONS **9,601** CITATIONS
SEE PROFILE

Comparative Analysis of Surface-Enhanced Raman Spectroscopy of Daidzein and Formononetin

Ryo Sekine,[†] Jitraporn Vongsvivut,[†] Evan G. Robertson,[‡] Leone Spiccia,[†] and Don McNaughton*,[†]

School of Chemistry, Monash University, Wellington Road, Clayton, Victoria 3800, Australia, and Department of Chemistry, La Trobe University, Bundoora, Victoria 3086, Australia

Received: February 15, 2010; Revised Manuscript Received: April 19, 2010

Phytoestrogens daidzein (4′,7-dihydroxy-isoflavone) and formononetin (4′-methoxy-7-hydroxy-isoflavone) have been studied by surface-enhanced Raman (SER) spectroscopy. Spectra were acquired in the presence of citrate-reduced silver colloids, over a range of pH and concentrations. Density functional theory calculations were used to assist assignment of the normal Raman spectra and help determine the mode of interaction of isoflavones with the silver nanoparticles. Formononetin does not show SER activity unless the 7-OH group is deprotonated, and accordingly, the interaction with the silver surface occurs via the deprotonated site. Daidzein, on the other hand, appears to contain multiple species at the surface, interacting via both the hydroxyl groups at 7-OH and 4′-OH, after deprotonation. This is an important result that points to potential future SERS applications in phytoestrogen analysis and provides a foundation for understanding the SER spectra of isoflavones.

Introduction

Surface-enhanced Raman spectroscopy (SERS) is a technique that has been found to provide large enhancements of Raman signals by factors of 10^6-10^{14} for molecular targets placed on the surface of roughened metal surfaces or nanoparticles.[1−3] While single molecule detection has been achieved for several target analytes using metal colloids,[4,5] the conditions are, in many cases, specific to a particular target and need to be determined by experiment to achieve the greatest, if any, enhancement. Furthermore, the theoretical basis of the phenomenon is complex and is a topic of continuing focus in SERS research.[6] These are some of the major factors that have prevented the widespread use of SERS. It is therefore necessary to study specific target molecules to define the parameters for SERS analysis and to broaden the available range of SERS active molecules and hence further our understanding.

In this paper, we examine two molecules that belong to a class of phytochemicals known as phytoestrogens. Phytoestrogens are chemicals found in plants that are receiving increasing attention in today's society with the growing awareness of their role in human health and diet; a number of potential health benefits have been identified, including the prevention or reduced risk of cancer, heart disease, osteoporosis, and postmenopausal symptoms.[7−11] On the other hand, some studies indicate that phytoestrogens may also have potentially adverse effects at high doses by acting as endocrine disrupting chemicals,[12,13] and they have been associated with various thyroid disorders[14] and impaired fertility,[15] particularly in males. Owing to these contrasting health effects of phytoestrogen-containing foods, techniques mostly based on UV−visible spectrophotometry or mass spectrometry have been developed to determine phytoestrogen content,[16−18] but there is considerable interest in developing alternative, rapid analytical techniques with potentially lower detection limits. The aim of this study is to lay the framework for the future application of SERS to phytoestrogen analysis.

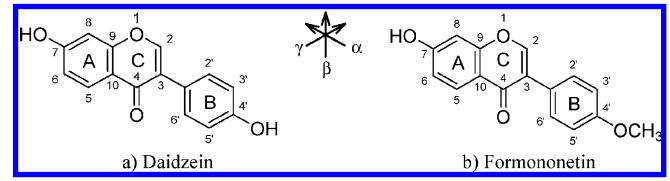

Figure 1. Molecular structures of the two isoflavones studied: (a) daidzein and (b) formononetin. The directions α, *β*, and *γ* refer to the directions used for defining the vibrational ring modes.

Of the range of natural phytoestrogens, isoflavones are a commonly encountered group in the human diet and are found in high concentrations in soy beans and other legumes. Daidzein (4′,7-dihydroxy-isoflavone) and formononetin (4′-methoxy-7-hydroxy-isoflavone) are two such examples with structures as shown in Figure 1. Isoflavones are characterized by the pendant aromatic ring (B) attached at the C_3 position of the chromone system (AC). A group of structurally related molecules, called flavones, have the pendant ring attached at the C_2 position of the chromone system and have been the subject of recent SERS studies reported by Teslova et al.[19] and by Jurasekova et al.[20] In contrast, to the best of our knowledge, there are no detailed SERS studies of isoflavones found in the literature, with only a brief report by Zhang et al.[21] on daidzein (in Chinese), and very recently, a quantitative assessment of a new SERS substrate has been published, which includes daidzein and genistein (4′,5,7-trihydroxy-isoflavone) as test environmental analytes to demonstrate its potential.[22] The lack of effective, reproducible, and reusable SERS substrates is another difficulty in SERS that precludes its use in routine analysis, and research to solve this problem is an active field in itself.[23−26]

Since the greatest spectral enhancement is observed from molecules at the metal surface, fundamental studies of the interaction of isoflavones with the metal surfaces are essential in optimizing methods in future applications. To this end, we

* Author to whom correspondence should be addressed. Tel.: +61-3-9905-4552. Fax: +61-3-9905-4597. E-mail: don.mcnaughton@sci.monash.edu.au.
[†] Monash University.
[‡] La Trobe University.

10.1021/jp101389t
Published on Web 05/05/2010

have recorded and assigned the normal Raman spectra of these isoflavones aided by density functional theory (DFT) calculations, optimized the conditions for SERS, and provisionally assigned the SERS by comparison with DFT calculations including a metal binding center. The molecular orientation of the phytoestrogen molecules adsorbed on the metal surface is explored through the SERS spectral features and vibrational band assignments.

Experimental Section

Materials and Reagents. Daidzein (≥99%) and formononetin (≥99.0%) were purchased from LC Laboratories (MA, USA) and Sigma-Aldrich (New South Wales, Australia), respectively, and were used without further purification. Stock solutions of 2.0 mM concentration were made in absolute ethanol (≥99.7% purity; Merck, Victoria, Australia), and working standards (10−100 μM) were prepared by further dilution of the stock solution.

All glassware was cleaned by treatment with either aqua regia (HNO_3 + HCl, 1:3 v/v) or a 10% Pierce PCC-54 detergent solution (Thermo Fisher Scientific Inc., IL, USA), an alternative recently reported to be as effective as aqua regia in cleaning the glassware for SERS purposes.[19,27] Glassware washed by the latter method was also subsequently sonicated for 5 min each in acetone and methanol and finally rinsed with 18.2 MΩ ultrapure water. No obvious changes in the spectra obtained from solutions prepared in glassware washed in either of the procedures could be identified.

Silver (Ag) colloids used in the SERS measurements were prepared by reduction of silver nitrate (≥99.9999% $AgNO_3$; Sigma-Aldrich, New South Wales, Australia) with citrate as reported by Lee and Meisel,[28] and the preparation specific to this paper is described elsewhere.[29] The absorption spectrum was measured periodically to monitor the colloid aggregation during synthesis. The colloid thus prepared had a turbid gray appearance with a λ_{max} = 408 nm, corresponding to Ag nanoparticles of ∼40 nm radius according to Mie theory.[30] Equally consistent SER spectra could be acquired after storage for several months even when λ_{max} of the colloid solution shifted as far as 413 nm.

Raman Spectroscopy and SERS Acquisition. All Raman and SERS measurements were carried out on a Renishaw Raman Microspectrometer RM2000 (Renishaw, New Mills, UK) equipped with a 782 nm NIR excitation laser and a thermoelectrical cooled CCD detector. Although fluorescence is reported to be insignificant from many isoflavonoids in the red-NIR regions,[31] it was found that changing to 633 nm excitation produced a broad and intense background. To avoid this fluorescence, and in consideration of the sensitivity of the samples toward photodegradation, the 782 nm laser excitation was employed in these experiments. The normal Raman (NR) spectra were obtained from the powder samples as purchased with ca. 5 mW laser power measured at the sample.

SER spectra were obtained in a manner very similar to that reported by Teslova et al.[19] Briefly, the spectra were acquired from a drop of premixed 2:1:2 Ag colloid solution:sample solution (10−100 μM):0.2 M aqueous solution of aggregating agent, with the laser focused by a 20× or 50× objective on the aggregates identified in the droplet. This aggregate formation and targeting was found to be critical in obtaining optimal SERS signals. The laser power measured at the sample for SERS was typically less than 1 mW, with 1 × 10 s accumulation, and the spectra presented are averages of spectra acquired from at least three different aggregates. Each individual spectrum was preprocessed by a three-step process prior to averaging: vector normalization over 1800−200 cm^{-1} followed by baseline correction and, finally, min−max normalization using the respective marker bands (795 cm^{-1} for daidzein and 1219 cm^{-1} for formononetin). This was necessary to account for resonance variation between different aggregates, which affect the absolute scattering intensities. Nitrate (NO_3^-, as KNO_3), sulfate (SO_4^{2-}, as Na_2SO_4), sulfite (SO_3^{2-}, as Na_2SO_3), disulfite ($S_2O_5^{2-}$, as $Na_2S_2O_5$), chloride (Cl^-, as NaCl), and perchlorate (ClO_4^-, as $NaClO_4$) were tested as aggregating agents in the study. For daidzein, it was found that SO_4^{2-} and NO_3^- gave equally good spectra, but NO_3^- was chosen to be consistent with previous work reported by other groups.[19,20] Where pH dependence of SERS activity was studied, the pH of the 0.2 M KNO_3 aggregating agent was varied by diluting a 0.2 M nitric acid solution with 0.2 M KNO_3 to keep the nitrate concentration constant over the series (pH range 3.2−12.2 at 1−2 pH unit intervals). Alkaline solutions were prepared by diluting a 0.2 M KOH solution with 0.2 M KNO_3. The analyte was added following the addition of the acid or base (which also contained the aggregating agent) so that the metal−analyte interaction would initiate at the desired pH. For formononetin, SO_4^{2-} was found to be the most suitable aggregating agent, and the pH was varied using addition of a suitable amount of 2×10^{-2} M H_2SO_4 or 5×10^{-3} M NaOH solution. Note that the reported pH for each spectrum is the pH of the final SERS mixture, which contains 20% ethanol (v/v) as solvent for the analytes. The increase in the value of pH as a result of the addition of the organic component was typically less than 0.3 pH units, which was much smaller than the pK_a of the two OH groups in daidzein.

Computational Chemistry. To assign the observed vibrational bands, normal vibrational modes and the Raman activities of the molecules' lowest-energy conformations were predicted by computational methods. Torsional angles were defined between the two ring systems AC and B as well as the pendant hydroxyl groups, and preliminary conformational searches were performed using the Hyperchem software (Version 8.0.4, Hypercube Inc., Gainesville FL, USA) at the AM1 semiempirical level. The four stable conformers were subsequently optimized using density functional theory (DFT) calculations using the Gaussian 03 software[32] (Gaussian, Inc., Wallingford CT, USA) at the B3LYP level with 6-31+G* basis set. This basis set was chosen to be consistent with previously reported work on structurally similar molecules,[19] where B3LYP/6-31+G* was selected as a compromise between accuracy and computational cost. For calculations on systems containing silver (Ag^0) atoms or ions (Ag^+), a mixed basis set was used where the 6-31+G* basis set was used for carbon, hydrogen, and oxygen, and the SDD basis set was used with Stuttgart pseudopotentials[33] for Ag^0 or Ag^+. Normal mode vibrations and Raman activities were computed on the final optimized structures and were used to simulate the experimental spectra, where the final intensities are calculated for 782 nm excitation (ν_0 = 12 787 cm^{-1}) using the formula[34]

$$I_i = \frac{f(\bar{\nu}_0 - \bar{\nu}_i)^4 S_i}{\bar{\nu}_i\left[1 - \exp\left(-\frac{hc\bar{\nu}_i}{kT}\right)\right]} \quad (1)$$

where S_i is the calculated Raman activity for the ith mode at $\bar{\nu}_i$ (cm^{-1}); h, c, and k are the fundamental constants; and f is a normalization factor. The temperature T was assumed to be 298 K.

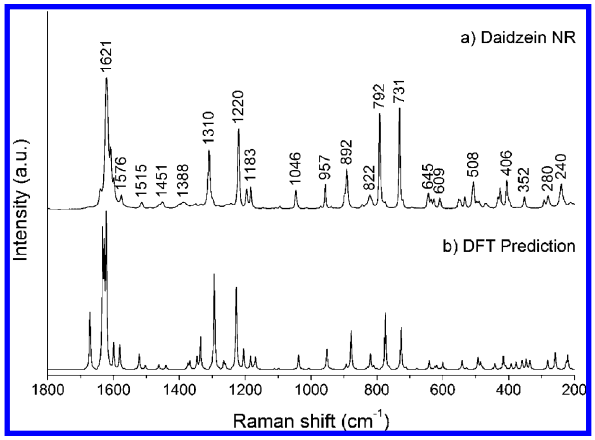

Figure 2. Experimental Raman (a) and DFT predicted (b) spectra of daidzein.

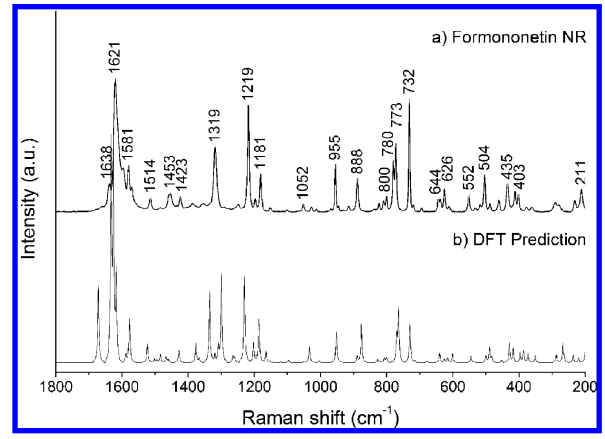

Figure 3. Experimental Raman (a) and DFT predicted (b) spectra of formononetin.

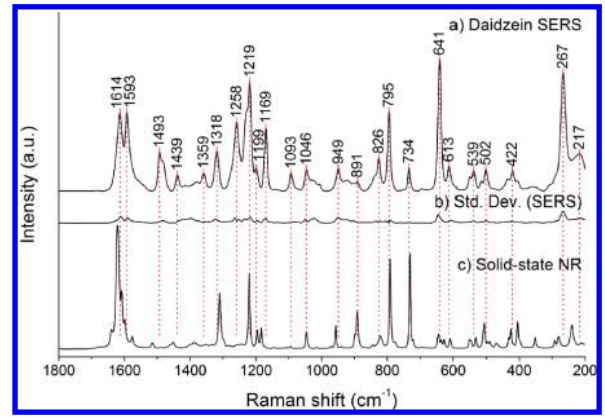

Figure 4. Comparison of an average SER spectrum (a), its standard deviation spectrum (b), and normal Raman spectrum (c) of daidzein. The pH of the SERS mixture is 8.3, and the final concentration is 5.1 ppm.

Results and Discussion

Normal Raman Spectra and Computational Chemistry Analysis. All optimized isoflavone structures had a nonplanar arrangement of the two ring systems AC and B, with inter-ring torsional angles for the lowest-energy conformers of daidzein and formononetin of 41° and 40°, respectively. This torsional angle was largely unaffected by deprotonation or metal attachment at the 7-OH in both daidzein and formononetin ($\Delta\tau \leq 2°$), while modifications at the 4′-OH in daidzein led to more significant changes toward a more coplanar arrangement ($\Delta\tau \leq 10°$). Subsequent vibrational frequency computation returned no negative wavenumbers, indicating the optimized geometries of these molecules are indeed minima on the potential energy surface.

The computed normal Raman spectrum of the lowest-energy conformer of daidzein is in good agreement with the experimentally obtained spectrum (Figure 2), and a detailed description of the normal modes is presented in the Supporting Information (Table S1). The predicted wavenumber values were uniformly scaled by a scaling factor (SF) of 0.979 evaluated using the least-squares method (combined with the formononetin data set) to give the minimum rms error of 11.9 cm^{-1} when compared against the experimental values. Such scaling factors have been found to be necessary when predicting vibrational frequencies to correct for, among several factors, anharmonicity of the potential energy surface.[35] In the case of formononetin, the Raman spectrum computed from the second most stable conformer was found to be in slightly better agreement with the experimental Raman spectrum, as evidenced by spectral features such as the 780−773 cm^{-1} doublet, as well as an rms error of 11.3 cm^{-1} compared to 11.8 cm^{-1}. Since they were very close in energy ($\Delta E = 0.25$ kJ·mol^{-1}), for simplicity, this conformer was ultimately used in the vibrational mode assignments and is presented in Figure 3. For consistency, predicted wavenumbers on all subsequent structures were scaled using the same factor of 0.979.

Surface-Enhanced Raman Spectroscopy of Daidzein and Formononetin. The critical step in successfully enhancing the Raman scattering in SERS is the adsorption of the analyte to the metal surface. In the unmodified citrate reduced silver colloids, the silver nanoparticles are coated with a layer of citrate introduced in the colloid preparation as the reducing agent[36] and hence have a negative surface charge (−48 mV at pH 6).[37] An anionic analyte, therefore, must surpass citrate in its affinity toward the metal surface for successful SERS observation, described as the competitive binding of anions by Bell et al.[38]

Daidzein and formononetin possess hydroxyl groups that can deprotonate and form various anionic forms. The first deprotonation has been established to occur at the 7-OH site in Ring A (see Figure 1), and pK_a values have previously been determined (pK_{a1} = 7.5 for daidzein and pK_a = 7.4 for formononetin).[39] Given that the pH of the citrate-reduced silver colloid after synthesis was found to be 9.1, it is expected that the anionic species would dominate over the neutral form when these samples are introduced into the colloid system.

Figure 4 shows a comparison of the normal Raman spectrum and typical SER spectrum of daidzein in the region between 1800 and 200 cm^{-1}. This spectrum is an average of spectra acquired from four different aggregates formed in the SERS-active solution, which was prepared by adding 50 μL of 0.2 M KNO_3 solution to 50 μL of the colloid solution, followed by the addition of 25 μL of 100 μM daidzein solution, resulting in a final pH of 8.3. As expected, there was considerable variation in the absolute SER intensities observed from different aggregates (~25%), but the relative intensities for the bands within each spectrum were very similar. The standard deviation spectrum calculated from the normalized, baseline corrected individual spectra is also included in Figure 4 to show the reproducibility of the obtained SERS profile. At first glance, the SER spectrum of daidzein reveals a good correlation of the positions of the major bands to the solid-state NR spectrum. However, it does exhibit a significant change in the relative intensity of the bands in comparison to the NR spectrum. As well as the strong bands at 1219 (NR: 1220), 795 (792), and 734 (731) cm^{-1}, which are prominent in both spectra, the SER

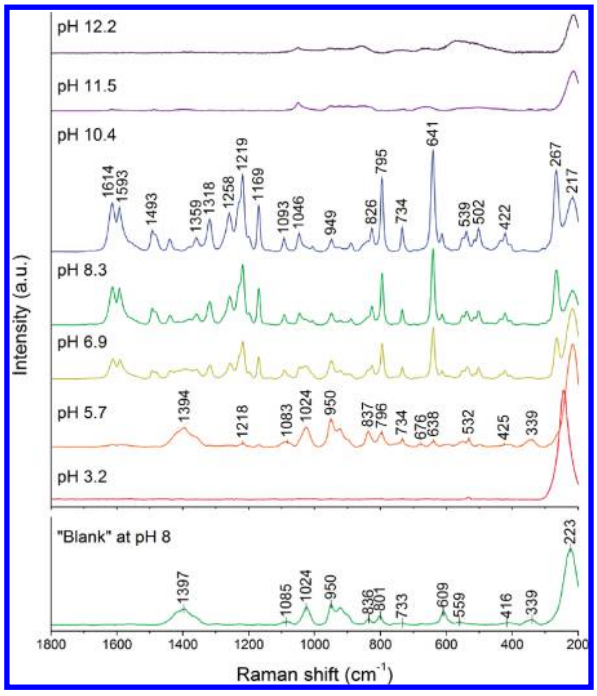

Figure 5. SER spectrum of daidzein (5.1 ppm) at various indicated pH values. Citrate peaks dominate at lower pH, while daidzein peaks appear at higher pH. The "blank" is that of the SERS mixture prepared with the solvent, but without daidzein, showing the characteristic features of citrate.

spectrum features intense bands at 1593, 1493, 1258, 1169, 641, and 267 cm^{-1}. This spectrum could reproducibly be obtained at subparts per million concentrations, and no significant, consistent changes were observed as the concentration was lowered.

At pH 8.3, over 80% of the analyte in the initial SERS mixture would be expected to be in its monoanionic form. As the pH of this SERS mixture is lowered, the analyte signal decreases, and the background citrate signals begin to dominate (Figure 5). This result clearly illustrates the pH-dependent nature of daidzein SER activity. As shown in Figure 5, the dramatic change in the spectral features observed from pH 5.7 to 8.3 suggests that daidzein needs to be in the deprotonated form to surpass the citrate affinity and adsorb onto the metal surface.

For comparison, the SER spectrum of the residual citrate is also shown in Figure 5. This was acquired by replacing the 100 μM daidzein solution in the SERS-active solution with the blank solvent (ethanol). The final pH of this solution was 8.0, which is in the SERS active range of daidzein. Since there is no significant difference in this spectrum and that containing daidzein at pH 5.7, it is unlikely that either the citrate or the silver surface itself is responsible for the observed pH dependence of the SERS activity of daidzein.

The second hydroxyl group of daidzein, the 4′-OH (see Figure 1), has a pK_{a2} of 9.65.[39] However, no significant changes in the spectral features were observed when the pH was increased to 10.4 or indeed until further increase to above pH 11, where the SER signal was lost, possibly due to OH^- competing for surface sites at higher concentrations and/or the formation of silver oxide species on the silver nanoparticle surface. Several weak bands can be observed (e.g., 1050 cm^{-1}, likely due to NO_3^-), but they do not correspond to daidzein. This indicates that either the same species is responsible for the SER spectrum over the entire pH range or that the relative population of each species in equilibrium at the surface is unaffected by the pH range

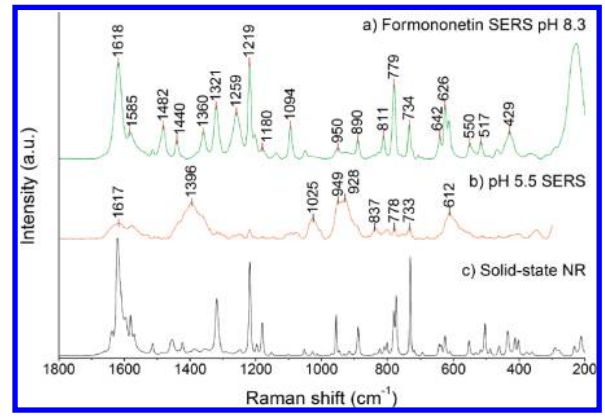

Figure 6. Comparison of the SER spectrum (a) at pH 8.3 (5.4 ppm) and (b) at pH 5.5 and (c) the normal Raman spectrum of formononetin.

investigated. Unfortunately, as the Raman spectra of the anionic forms of the isoflavones have not been obtained for practical reasons, direct comparisons cannot be made, but the simulated Raman spectra of daidzein (available as Supporting Information, Figure S1) in its neutral and deprotonated forms reveal that the majority of the normal mode vibrations are very similar. Single deprotonation at 7-OH results in only small wavenumber shifts, and relative intensity changes are observed in the lower wavenumber region, while both position and intensity change significantly in the aromatic stretching regions (>1350 cm^{-1}) where OH bending and ring stretching vibrations are coupled in the normal modes.

As a comparison, the SER spectrum of formononetin, the 4′-methoxy derivative of daidzein, was acquired and analyzed. In a manner to similar daidzein, the spectral features that are prominent at acidic pH are again those of surface citrate, and the analyte characteristics begin to appear as the pH is increased (Figure 6), thus confirming the critical nature of analyte deprotonation for SERS observation. The SER spectrum could be observed even at subparts per million (<0.3 ppm) concentrations without difficulty. Since formononetin can deprotonate only at the 7-OH site, it follows that this is the likely site of interaction.

It is interesting to note at this stage that the normal Raman spectra of daidzein and formononetin are very similar by both experiment and theory, with the majority of the bands appearing in the same positions. On the other hand, the experimental SER spectra of the two are significantly different, and from an analytical application perspective, the SER spectra may therefore be more useful in accurately distinguishing between the two species.

Comparison of the Analyte−Metal Interactions and Further Discussions. According to the surface selection rules, vibrational modes with polarizability components perpendicular to the metal surface are enhanced to the greatest extent.[40] Thus, systematic analysis of the enhanced modes provides insights into the orientation of the molecule at the surface of the metal. Since daidzein and formononetin adsorb on the metal surface after deprotonation to give the SER spectrum, a direct comparison of the relative intensities with the NR spectrum, which is in the neutral form, would be inappropriate. Furthermore, Raman intensities calculated using DFT have been found to be inaccurate in some studies,[41] and thus a stringent calculation of enhancement factors for every vibrational mode would not be justified.

A useful approach that has been employed to study the analyte−metal interaction is the addition of a metal center onto the analyte interaction site.[42,43] While this simple model cannot

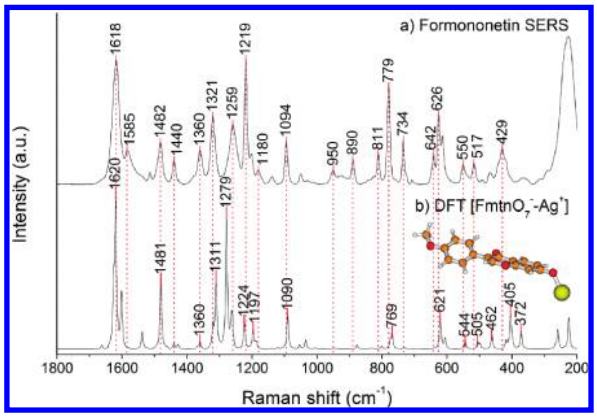

Figure 7. Comparison of (a) the experimental SER spectrum of formononetin (5.4 ppm) and (b) the simulated Raman spectrum of the deprotonated formononetin−Ag^+ complex, [$FmtnO_7^-$−Ag^+] (optimized structure shown).

provide an accurate description of the local electric field (since plasmons are a result of electrons from a larger collection of atoms) and the intensities will therefore be inaccurate, a qualitative assessment of the mode of interaction can be arrived at from the predicted wavenumber shifts of major bands. In this case, since the SER spectrum of the two isoflavones began to appear over the pH range where the 7-OH would deprotonate, the silver metal center (Ag^0 or Ag^+) was attached to the resultant negatively charged 7-O^-. Geometry optimized structures of the formononetin anion−silver complex [$FmtnO_7^-$−Ag^+] have a Ag^+−O^- bond distance of 2.08 Å and an Ag^+−O^-−C_7 angle of 120−124°, depending on the dihedral angle about Ag^+−O^-−[Ring A]. Several stationary points were found with respect to this dihedral degree of freedom, and the lowest-energy structure had the silver lying in the plane of rings AC; however, the electronic energy varied by no more than 4 kJ/mol, which is insignificant compared to the various intermolecular interactions that may be occurring. The best overall match in the appearance of the predicted spectrum was obtained from a complex with bond length, angle, and torsion of 2.08 Å, 124°, and 112°, respectively (Figure 7). The rms error for the major bands assigned in Table 1 was 8.92 cm^{-1}. The deprotonated daidzein−Ag^+ complex ([$DznO_7^-$−Ag^+]), where the interaction is via an Ag^+−O^- bond with the deprotonated oxygen, yielded results very similar to formononetin. There are again several stationary points with various Ag^+−O_7^-−[Ring A] torsions, while there was little variation in the Ag^+−O^- bond length (2.08 Å) and the Ag−O−C_7 angle (120−124°). Not surprisingly, the spectra calculated for [$DznO_7^-$−Ag^+] and [$FmtnO_7^-$−Ag^+] are very similar.

TABLE 1: SERS Band Assignments for Formononetin Using the Results of DFT Calculations on the Deprotonated Formononetin−Ag^+ Complex, Their Descriptions, and Their Corresponding Positions in the Neutral, Isolated Formononetin Molecule

experimental (cm^{-1})[a]					DFT prediction (cm^{-1})[b]			
SERS[a]		NR[a]		Δ	[$FmtnO_7^-$−Ag^+]	Fmtn.	Δ	description of [$FmtnO_7^-$−Ag^+] mode[c]
					372	−	−	ν(Ag−O_7) + δ($C_3C_1'C_2'$)
429	m	413	m	17	405	397	8	τ($C_9O_1C_2C_3$) + τ($C_7C_8C_9C_{10}$) + ν(Ag−O_7)[g]
468	w	461	w	7	462	454	8	δ($C_3'C_4'O$) + τ($C_9C_{10}C_5C_6$) + τ($O_1C_2C_3C_1'$)[g]
517	m	518	m	−1	505	500	5	δ(C_6C_7O) + δ($O_1C_9C_8$) + δ($C_4'OC_{Me}$) + ν(Ag−O_7)
550	m	552	m	−2	544	545	−1	δ($C_2C_3C_4$) + $\gamma(CCC)^{16b\ h}_{B\alpha}$ + $\delta(CCC)^{6a}_{A\gamma}$
614	m	612	w	2	606	601	5	δ(C_4=O) + δ(OC_7C_8) + δ($C_1'C_3C_4$)
626	s	626	m	0	620	616	4	δ($C_2'C_3'C_4'$) + δ($C_4'OC_{Me}$)
642	m	644	w	−2	639	640	−1	$\delta(CCC)^{6b}_{B\alpha}$
734	s	732	vs	2	731	730	1	$\delta(CCC)^{6a}_{A\beta}$
779[d]	*vs*	773	s	6	769	764	5	τ($C_1'C_3C_4$=O) + τ($C_4'C_5'C_6'$H) + δ($C_6'C_1'C_2'$)[g]
		780	s	−1	774	770	−6	τ($C_1'C_3C_4$=O) + τ($C_9C_{10}C_5$H)[g]
811	m	800	m	12	801	800	1	$\gamma(C-H)^{10a}_{B\alpha}$
890	m	888	s	2	877	877	0	δ($O_1C_2C_3$) + δ(C_4=O) + $\delta(CCC)^{1}_{B}$
950[e]	w	955	s	−6	949	952	−3	ν_{sym}(C_6−C_7, C_7−C_8)
1050	w	1052	m	−2	1054	1052	2	ν(C_{Me}−O)
1094	s	1101	*vw*	−7	1090	1097	−7	$\delta(C-H)^{18a}_{A\alpha}$ + ν_{sym}(O_1−C_9, O_1−C_2)
1138	w	−		−	−	−	−	
1180	w	1181	s	−1	1186	1186	0	$\delta(C-H)^{9a}_{B\alpha}$ + δ($O_4'C_{Me}H_{IP}$)
1203	m	1197	w	6	1197	1203	−6	δ(C_8−H) + ν_{asym}(O_1−C_2, C_4−C_{10})
1219	vs	1219	vs	1	1224	1230	−6	δ(C_5−H) + δ(C_8−H) + ν(O_1−C_2) + ν(C_5−C_{10}) + ν(C_3−C_1')
1259	s, br	1319[f]	s	−60	1279	1300[f]	−21	ν(C_7−O) + δ(C_5−H) + δ(C_6−H)
1321	s	−		−	1311	−	−	ν(C_3−C_1') + δ(C_2−H) + $\delta(C-H)^{9b}_{B\alpha}$ + ν_{sym}(C_9−C_{10}, C_7−C_8)
1360	m	−		−	1360	1377	−17	ν(O_1−C_9) + δ(C_2−H) + $\nu(C=C)^{14}_{A}$
1440	m	1460	*w*	−20	1441	1467	−26	$\nu(C=C)^{19b\ h,i}_{A\alpha}$
1482	s	−		−	1481	1502	−21	$\nu(C=C)^{19a\ h,i,j}_{A\alpha}$
1514	w	1514	w	0	1523	1523	0	$\nu(C=C)^{19a\ h,i}_{B\alpha}$
1585	m	1571	w	14	1581	1578	3	$\nu(C=C)^{8b}_{B\beta}$
1618	vs	1621	vs	−3	1620	1633	−13	ν(C_2=C_3) + $\nu(C=C)^{8a\ h}_{A\alpha}$

[a] Labels used: vs, very strong; s, strong; m, medium; w, weak; and vw, very weak; also br, broad and sh, shoulder. [b] All DFT predicted wavenumbers have been scaled uniformly by a factor of 0.979. [c] Notations used: ν = stretch, δ = in plane bend, γ = out of plane bend, τ = torsion. Where a ring mode closely resembles those of benzene as shown by Alcolea Palafox,[51] Wilson numbering of the mode (1−20b) is shown in the superscript following a general description of the mode in parentheses, while the subscript indicates the corresponding ring (A, B, or C) and, where applicable, direction (α, β, or γ as in Figure 1). Some modes are slightly different due to oxygen being significantly heavier than hydrogen. [d] Two peaks in the NR likely to have merged into a single unresolved peak in SERS. [e] Some contribution from the overlapping citrate band is likely to be present. [f] ν(C_7−O) is coupled to ν(C_3−C_1') in the neutral formononetin into symmetric and antisymmetric modes. The symmetric mode is adopted here. [g] Torsional components (independent) experiencing the largest displacements according to the Gaussian 03 Program output are listed. [h] The motions appear as (CCC + CH). [i] Vibration degenerate according to Scherer. [j] Some ν(C_7−O) component present.

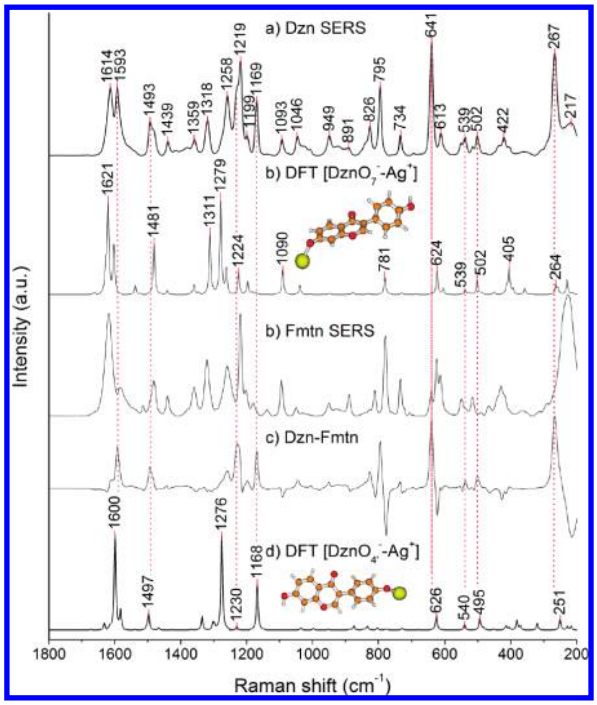

Figure 8. Comparison of (a) the SER spectrum of daidzein (5.1 ppm), (b) predicted Raman spectrum of the 7-OH deprotonated daidzein−Ag^+ complex, [$DznO_7^-$−Ag^+], (c) SERS of formononetin (5.4 ppm), (d) SER spectrum of daidzein subtract formononetin, and (e) predicted Raman spectrum of the 4′-OH deprotonated daidzein−Ag^+ complex, [$DznO_{4'}^-$−Ag^+]. The remnant bands in the difference spectrum (d) align well with the [$DznO_{4'}^-$−Ag^+] spectrum.

On the contrary, as noted earlier, the experimental SERS profiles of the two isoflavones have several distinct differences. There is a better overall agreement in appearance between the predicted spectrum of the metal complex and the experimental SER spectrum of formononetin than there is with daidzein. This suggests that daidzein may be interacting with the silver surface in a slightly different manner, which would also justify the use of different aggregating agents. Various deprotonation patterns and Ag^0/Ag^+ interactions were modeled with DFT in an attempt to reduce the discrepancy, but no single predicted spectrum convincingly reproduced the experimental spectrum. However, upon comparing the SER spectra of the two, it appears that the SER spectrum of daidzein actually has many overlapping bands with that of formononetin. It can be recognized as almost identical to the formononetin spectrum but with several additional peaks: 1593, 1493, 1231 (shoulder to 1219 cm^{-1} assigned by second derivative spectrum), 1169, and 641 cm^{-1}, as can been seen by the difference spectrum (Dzn-Fmtn) in Figure 8. In fact, when compared with the predicted spectra, the peaks in common can be satisfactorily assigned to [$DznO_7^-$−Ag^+], while the "extra" peaks correspond to the major peaks that are predicted in the 4′-OH deprotonated form [$DznO_{4'}^-$−Ag^+]: 1600, 1497, 1230, 1168, and 626 cm^{-1}. It therefore seems likely that various anionic forms of daidzein may exist to produce the acquired SER spectra. As further evidence, the band at 1259 cm^{-1}, assigned to the C−O^- stretching mode, is more intense in the daidzein spectrum than in the formononetin spectrum. Since the spectra were normalized against peaks that are predicted with the 7-OH deprotonated forms, the difference in the intensity of this band must originate

TABLE 2: SERS Band Assignments for Daidzein Using the Results of DFT Calculations on the 7-OH or 4′-OH Deprotonated Daidzein−Ag^+ Complexes, Their Descriptions, and Their Corresponding Positions in the Neutral, Isolated Daidzein Molecule

experimental (cm^{-1})[a]					DFT prediction (cm^{-1})[b]				
SERS		NR		Δ	[D_7−Ag^+]	[$D_{4'}$−Ag^+]	Dzn	Δ	description of [$DznO_7^-$−Ag^+] or [$DznO_{4'}^-$−Ag^+] mode[a]
267	vs	292	w	−25	264		282	−18	$\tau(C_5C_6C_7O) + \tau(C_9C_{10}C_4{=}O) + \tau(C_8C_9O_1C_2)$[e]
						320	−	−	$\nu(Ag{-}O_4')$
					358		−	−	$\nu(Ag{-}O_7)$
422	m	396	w, sh	26	405		377	28	$\tau(C_9O_1C_2C_3) + \delta(C_8C_7O) + \nu(Ag{-}O_7)$
502	m	508	m	−6		495	493	2	$\delta(CCC)^{6a}_{C\beta} + \nu(Ag{-}O_4')$
515	w			7	502			9	$\delta(C_6C_7O) + \delta(O_1C_9C_8) + \delta(CCC)^{6a}_{C\beta} + \nu(Ag{-}O_7)$
539	m	551	w	−12		540	542	−2	$\gamma(CCC)^{16b}_{B\alpha} + \delta(C_2C_3C_4) + \delta(CCC)^{6a}_{A\gamma} + \nu(Ag{-}O_4')$
551	w			0	539			−1	$\gamma(CCC)^{16b}_{B\alpha} + \delta(C_2C_3C_4) + \delta(CCC)^{6a\,f}_{A\gamma}$
613	m	609	w	4	605		600	5	$\delta(C_4{=}O) + \delta(OC_7C_8) + \delta(C_1'C_3C_4)$
641	vs	628	w	13	624		619	5	$\delta(C_3'C_4'C_5') + \delta(OC_9C_{10}) + \nu(C_3{-}C_1')$
						626		7	$\delta(C_3'C_4'C_5') + \delta(OC_9C_{10}) + \nu(C_3{-}C_1') + \nu(Ag{-}O_4')$
734		731	vs	3	731		727	4	$\delta(CCC)^{6a}_{A\beta} + \nu(C_9{-}O_1)$
795		792	vs	3	781		775	6	$\tau(C_1'C_3C_4{=}O) + \delta(C_2O_1C_9) + \nu(C_4{-}C_{10}) + \nu(C_3{-}C_4)$
826	m	822	w	4	820		820	0	$\delta(C_2'C_1'C_6') + \nu(C_4'{-}O) + \nu_{sym}(C_3'{-}C_4', C_4'{-}C_5')$
891	s	892	s	−1	877		878	−1	$\delta(O_1C_2C_3) + \delta(C_4{=}O) + \delta(CCC)^{1}_{B}$
949[c]	m	957	m	−8	949		952	−3	$\nu_{sym}(C_6{-}C_7, C_7{-}C_8) + \delta(C_5{-}H) + \tau(HC_2'C_3'H)$
1006	w	1013	vw	−7	1007		1007	0	$\delta(C{-}H)^{18a}_{B\alpha}$
1046	m	1046	m	0	1039		1038	1	$\nu(C_3{-}C_4) + \nu(O_1{-}C_2) + \nu_{sym}(C_1'{-}C_2', C_1'{-}C_6')$
1093	m	1095	vw	−2	1090		1098	−8	$\delta(C{-}H)^{18a}_{A\alpha} + \nu_{sym}(O_1{-}C_9, O_1{-}C_2)$
1169	s	1183	m	−14		1168	1184	−16	$\delta(C{-}H)^{9a}_{B\alpha}$
1199	w	1196	m	3	1197		1205	−8	$\delta(C_8{-}H) + \nu_{asym}(O_1{-}C_2, C_4{-}C_{10})$
1219	vs	1220	s	−2	1224		1227	−3	$\delta(C_5{-}H) + \delta(C_8{-}H) + \nu(O_1{-}C_2) + \nu(C_5{-}C_{10}) + \nu(C_3{-}C_1')$
1231	s,sh			11		1230		3	$\delta(C_5{-}H) + \delta(C_8{-}H) + \nu(C_3{-}C_1') + \nu(O_1{-}C_2) + \nu(C_5{-}C_{10})$
1258	*s*	1256	vw, br	2		1276	1265	11	$\nu(C_4'{-}O)$
		1310[d]	s	−52	1279		1294[d]	−15	$\nu(C_7{-}O) + \delta(C_5{-}H) + \delta(C_6{-}H)$
1318	m	1335	vw	−16	1311		1336	−25	$\delta(C_2{-}H) + \nu(C_3{-}C_1') + \nu_{sym}(C_9{-}C_{10}, C_7{-}C_8)$
1359	m	1388	vw, br	−29	1360		1375	−15	$\delta(C_2{-}H) + \nu(O_1{-}C_9) + \nu(C{=}C)^{14}_{A}$
1439	m	1463	w, sh	−24	1441		1462	−21	$\nu(C{=}C)^{19b}_{A\alpha} + \nu(C{=}C)^{19b\,f,g}_{B\alpha}$
1481	m, sh	1490	vw	−9	1481		1504	−23	$\nu(C{=}C)^{19a\,f,g,h}_{A\alpha}$
1493	m	1515	*w*	−22		1497	1522	−25	$\nu(C{=}C)^{19a\,f,g,h}_{B\alpha}$
1593	vs					1600	1628	−28	$\nu(C{=}C)^{8a\,f}_{B\alpha}$
1614	vs	1609	s, sh	5	1621		1622	−1	$\nu(C_2{=}C_3) + \nu(C{=}C)^{8a\,f}_{A\alpha}$

[a] Labels and Notations as per Table 1. [b] All DFT predicted wavenumbers have been scaled uniformly by a factor of 0.979. [c] Some contribution from the overlapping citrate band is likely to be present. [d] $\nu(C_7{-}O)$ is coupled to $\nu(C_3{-}C_1')$ in the neutral daidzein as per formononetin. [e] See Table 1. [f] The motions appear as (CCC + CH). [g] Vibration degenerate according to Scherer. [h] Some $\nu(C_7{-}O)$ or $\nu(C_4'{-}O)$ component. [i] Slightly different from NR.

from the $C_{4'}-O^-$ stretch contribution, predicted at 1276 cm^{-1} (1279 cm^{-1} for C_7-O^-), which would add to the intensity of this band. It should be noted that the bands at 795 cm^{-1} in daidzein and 779 cm^{-1} in formononetin were significantly offset even in the NR spectra (19 cm^{-1}), resulting in misaligned subtraction of this band as seen by the odd appearance in this region. The final rms value for band assignments (Table 2) from the combination of predicted spectra for the two possible interactions is 8.53 cm^{-1}.

It is important to re-emphasize that the nature of such differences in an attachment has significant consequences in the resultant spectra. The various deprotonation patterns and metal attachments produced DFT predicted spectra which exhibited not only some wavenumber shifts but also significant relative intensity changes, and such variation has also been observed in other SERS experiment studies, for example, by Canamares et al. with alizarin.[44] Thus, the different experimental conditions can have a pronounced effect on the resultant SER spectrum. It is therefore not surprising that our SER spectrum of daidzein is apparently inconsistent with that reported by Bhandari et al.,[22] which is again different from Zhang et al.,[45] given the vastly different experimental conditions employed (excitation laser frequency and intensity, nature of the SERS substrate, and the presence/absence of additional species in equilibria in the system). For example, the spectrum reported by Bhandari et al. was acquired from a silver-coated polypropylene filter in the dry phase after preconcentration and has a marker band at 837 cm^{-1} with the overall appearance distinctly different from our SER or NR spectra of daidzein. Degradation of the sample may also occur under certain conditions, for example, in highly alkaline solutions.[46] Sanchez-Cortes et al. revealed that chemical modification of phenol derivatives containing *o*-diphenol moieties (as in, for example, catechol) can occur at metal surfaces used for SERS,[47] and such degradation has been studied in detail for the flavone quercetin.[48] Neither daidzein nor formononetin possess the identified chemically labile groups, and given the good agreement with the DFT results, however inconclusive, it is unlikely that chemical degradation is taking place. Nevertheless, this highlights the necessity to perform fundamental studies in conjunction or prior to application to correctly interpret results and the need to carefully control the experimental conditions throughout a particular study (for example, in quantitative measurements). Conversely, exploiting the high sensitivity of the SERS profile to the nature of the analyte and its interactions at the metal surface may have potential applications in future in situ studies of isoflavones in plant or human physiology.

Finally, this research approach demonstrates the effectiveness of using DFT calculations to study molecular interactions observed in SERS through normal-mode analysis, also demonstrated recently in the study of the pesticide fonofos.[49] Furthermore, the simple addition of the metal centers into the calculations is able to provide significant qualitative insights into wavenumber shifts upon binding, without the use of higher-level methods such as time-dependent DFT (TD-DFT)[50] and the inclusion of metal clusters, which become necessary to model the SERS intensity enhancements.

Conclusions

Surface-enhanced Raman spectroscopy has been demonstrated for two common isoflavones: daidzein and formononetin. The pH-dependent studies on SERS of daidzein and formononetin have revealed that the two molecules need to be deprotonated to adsorb onto the silver surface and thereby to achieve effective Raman enhancements. While the formononetin anion only has one site of interaction at the negatively charged 7-O^-, daidzein, which has two possible sites at 7-O^- and 4′-O^-, appears to interact via both sites. Band assignments for the normal Raman as well as for SER spectra based on these interactions have been presented, assisted by DFT calculations. Future work will focus on examining other isoflavones with different substitution patterns and comparison of their modes of interactions.

Acknowledgment. We would like to thank the Australian Partnership for Advanced Computing National Facility (APAC) and the Monash Sun Grid at the Monash e-Research Centre for computational facilities, the Australian Government, and the Monash Research Graduate School (MRGS) for postgraduate scholarship support. We also acknowledge the invaluable assistance from Mr. Finlay Shanks with spectroscopic instrumentation and Mr. Mehdi Asghari Khiavi with computational calculations.

Supporting Information Available: A complete list of observed Raman bands of daidzein (Table S1) and formononetin (Table S2) together with the normal mode descriptions as assigned with DFT and a graphic comparison of the Raman spectra predicted using DFT on daidzein and its anionic forms (Figure S1). This material is available free of charge via the Internet at http://pubs.acs.org.

References and Notes

(1) Fleischmann, M.; Hendra, P. J.; McQuillan, A. J. *Chem. Phys. Lett.* **1974**, *26*, 163.
(2) Albrecht, M. G.; Creighton, J. A. *J. Am. Chem. Soc.* **1977**, *99*, 5215.
(3) Jeanmaire, D. L.; Van Duyne, R. P. *J. Electroanal. Chem.* **1977**, *84*, 1.
(4) Nie, S.; Emory, S. R. *Science* **1997**, *275*, 1102.
(5) Kneipp, K.; Wang, Y.; Kneipp, H.; Perelman, L. T.; Itzkan, I.; Dasari, R. R.; Feld, M. S. *Phys. Rev. Lett.* **1997**, *78*, 1667.
(6) Lombardi, J. R.; Birke, R. L. *J. Phys. Chem. C* **2008**, *112*, 5605.
(7) Gültekin, E.; Yildiz, F. Introduction to Phytoestrogens. In *Phytoestrogens in Functional Foods*; Yildiz, F., Ed.; CRC Press: Boca Raton, 2006; p 3.
(8) Karahalil, B. Benefits and Risks of Phytoestrogens. In *Phytoestrogens in Functional Foods*; Yildiz, F., Ed.; CRC Press: Boca Raton, 2006.
(9) Jackman, K. A.; Woodman, O. L.; Sobey, C. G. *Curr. Med. Chem.* **2007**, *14*, 2824.
(10) Morrissey, C.; Watson, R.; G., W. *Curr. Drug Targets* **2003**, *4*, 231.
(11) Usui, T. *Endocr. J.* **2006**, *53*, 7.
(12) McLachlan, J. A. *Endocr. Rev.* **2001**, *22*, 319.
(13) Wood, S. L.; Jarrell, J. J.; Swaby, C.; Chan, S. *Environ. Health* **2007**, *6*, 35.
(14) Divi, R. L.; Chang, H. C.; Doerge, D. R. *Biochem. Pharmacol.* **1997**, *54*, 1087.
(15) Strauss, L.; Santti, R.; Saarinen, N.; Streng, T.; Joshi, S.; Mäkelä, S. *Toxicol. Lett.* **1998**, *102−103*, 349.
(16) Wang, C. C.; Prasain, J. K.; Barnes, S. *J. Chromatogr. B* **2002**, *777*, 3.
(17) Vacek, J.; Klejdus, B.; Lojkova, L.; Kuban, V. *J. Sep. Sci.* **2008**, *31*, 2054.
(18) Thompson, L. U.; Boucher, B. A.; Liu, Z.; Cotterchio, M.; Kreiger, N. *Nutr. Cancer* **2006**, *54*, 184.
(19) Teslova, T.; Corredor, C.; Livingstone, R.; Spataru, T.; Birke, R. L.; Lombardi, J. R.; Cañamares, M. V.; Leona, M. *J. Raman Spectrosc.* **2007**, *38*, 802.
(20) Jurasekova, Z.; Garcia-Ramos, J. V.; Domingo, C.; Sanchez-Cortes, S. *J. Raman Spectrosc.* **2006**, *37*, 1239.
(21) Zielonka, J.; Gebicki, J.; Grynkiewicz, G. *Free Radical Biol. Med.* **2003**, *35*, 958.
(22) Bhandari, D.; Walworth, M. J.; Sepaniak, M. J. *Appl. Spectrosc.* **2009**, *63*, 571.
(23) Bao, L.; Mahurin, S. M.; Dai, S. *Anal. Chem.* **2004**, *76*, 4531.
(24) Farquharson, S.; Maksymiuk, P. *Appl. Spectrosc.* **2003**, *57*, 479.
(25) Wang, W.; Gu, B. *Appl. Spectrosc.* **2005**, *59*, 1509.
(26) Zhang, M.-L.; Fan, X.; Zhou, H.-W.; Shao, M.-W.; Zapien, J. A.; Wong, N.-B.; Lee, S.-T. *J. Phys. Chem. C* **2010**, *114*, 1969.
(27) Leona, M. *Proc. SPIE* **2005**, *5993*, 59930L.
(28) Lee, P. C.; Meisel, D. *J. Phys. Chem.* **1982**, *86*, 3391.

(29) Vongsvivut, J.; Robertson, E. G.; McNaughton, D. *Aust. J. Chem.* **2008**, *61*, 921.
(30) Aroca, R. *Surface-Enhanced Vibrational Spectroscopy*; John Wiley & Sons, Ltd.: West Sussex, England, 2006.
(31) Dunford, C. L.; Smith, G. J.; Swinny, E. E.; Markham, K. R. *Photochem. Photobiol. Sci.* **2003**, *2*, 611.
(32) Frisch, M. J.; Trucks, G. W.; Schlegel, H. B.; Scuseria, G. E.; Robb, M. A.; Cheeseman, J. R.; J. A. Montgomery, J.; Vreven, T.; Kudin, K. N.; Burant, J. C.; Millam, J. M.; Iyengar, S. S.; Tomasi, J.; Barone, V.; Mennucci, B.; Cossi, M.; Scalmani, G.; Rega, N.; Petersson, G. A.; Nakatsuji, H.; Hada, M.; Ehara, M.; Toyota, K.; Fukuda, R.; Hasegawa, J.; Ishida, M.; Nakajima, T.; Honda, Y.; Kitao, O.; Nakai, H.; Klene, M.; Li, X.; Knox, J. E.; Hratchian, H. P.; Cross, J. B.; Bakken, V.; Adamo, C.; Jaramillo, J.; Gomperts, R.; Stratmann, R. E.; Yazyev, O.; Austin, A. J.; Cammi, R.; Pomelli, C.; Ochterski, J. W.; Ayala, P. Y.; Morokuma, K.; Voth, G. A.; Salvador, P.; Dannenberg, J. J.; Zakrzewski, V. G.; Dapprich, S.; Daniels, A. D.; Strain, M. C.; Farkas, O.; Malick, D. K.; Rabuck, A. D.; Raghavachari, K.; Foresman, J. B.; Ortiz, J. V.; Cui, Q.; Baboul, A. G.; Clifford, S.; Cioslowski, J.; Stefanov, B. B.; Liu, G.; Liashenko, A.; Piskorz, P.; Komaromi, I.; Martin, R. L.; Fox, D. J.; Keith, T.; Al-Laham, M. A.; Peng, C. Y.; Nanayakkara, A.; Challacombe, M.; Gill, P. M. W.; Johnson, B.; Chen, W.; Wong, M. W.; Gonzalez, C.; Pople, J. A. *Gaussian 03*, revision E.01; Gaussian, Inc.: Wallingford, CT, 2004.
(33) Andrae, D.; Häuβermann, U.; Dolg, M.; Stoll, H.; Preuβ, H. *Theor. Chim. Acta* **1990**, *77*, 123.
(34) Krishnakumar, V.; Keresztury, G.; Sundius, T.; Ramasamy, R. *J. Mol. Struct.* **2004**, *702*, 9.
(35) Scott, A. P.; Radom, L. *J. Phys. Chem.* **1996**, *100*, 16502.
(36) Munro, C. H.; Smith, W. E.; Garner, M.; Clarkson, J.; White, P. C. *Langmuir* **1995**, *11*, 3712.
(37) Alvarez-Puebla, R. A.; Arceo, E.; Goulet, P. J. G.; Garrido, J. J.; Aroca, R. F. *J. Phys. Chem. B* **2005**, *109*, 3787.
(38) Bell, S. E. J.; Sirimuthu, N. M. S. *J. Phys. Chem. B* **2005**, *109*, 7405.
(39) Liang, J.; Tian, Y. X.; Fu, L. M.; Wang, T. H.; Li, H. J.; Wang, P.; Han, R. M.; Zhang, J. P.; Skibsted, L. H. *J. Agric. Food Chem.* **2008**, *56*, 10376.
(40) Moskovits, M. *J. Chem. Phys.* **1982**, *77*, 4408.
(41) Williams, S. D.; Johnson, T. J.; Gibbons, T. P.; Kitchens, C. L. *Theor. Chem. Acc.* **2007**, *2007*, 283.
(42) Cardini, G.; Muniz-Miranda, M.; Schettino, V. *J. Phys. Chem. B* **2004**, *108*, 17007.
(43) Vivoni, A.; Birke, R. L.; Foucault, R.; Lombardi, J. R. *J. Phys. Chem. B* **2003**, *107*, 5547.
(44) Canamares, M. V.; Garcia-Ramos, J. V.; Domingo, C.; Sanchez-Cortes, S. *J. Raman Spectrosc.* **2004**, *35*, 921.
(45) Zhang, J.; Wang, Y.; Zhang, X. *Chin. J. Chem. Phys.* **1998**, *11*, 211.
(46) Wang, S. F.; Ye, Y. H.; Zhang, Z.; Tan, R. X. *Ultrason. Sonochem.* **2006**, *13*, 28.
(47) Sanchez-Cortes, S.; Garcia-Ramos, J. V. *J. Colloid Interface Sci.* **2000**, *231*, 98.
(48) Jurasekova, Z.; Torreggiani, A.; Tamba, M.; Sanchez-Cortes, S.; Garcia-Ramos, J. V. *J. Mol. Struct.* **2008**.
(49) Vongsvivut, J.; Robertson, E. G.; McNaughton, D. *J. Raman Spectrosc.* **2010**, in press, 10.1002/jrs.2579.
(50) Zhao, L.; Jensen, L.; Schatz, G. C. *J. Am. Chem. Soc.* **2006**, *128*, 2911.
(51) Alcolea Palafox, M. *Int. J. Quantum Chem.* **2000**, *77*, 661.

JP101389T